

more reflectance techniques. (cite)

## II. THEORETICAL FORMULATION

### A. Vibrational Thermal Conductivity

We calculate the total vibrational thermal conductivity  $k_{vib}$  of amorphous solids, we predict the contributions from  $k_{pr}$  and  $k_{AF}$ , from

$$k_{vib} = k_{pr} + k_{AF}, \quad (1)$$

where  $k_{pr}$ <sup>35-37</sup> is the contribution from propagating (phonon-like) modes and  $k_{AF}$  is the non-propagating contribution from the Allen-Feldman (AF) theory of diffusors.<sup>14</sup> The form of Eq. (1) has been used in several previous studies of amorphous materials with varying assumptions.<sup>14-18,23,38</sup> The various assumptions all lead to predictions that  $k_{pr}$  is a negligible (< 10%) and non-negligible (> 20%) fraction of  $k_{vib}$  for a-SiO<sub>2</sub>(cite) and a-Si(cite), respectively.

The contribution  $k_{pr}$  is predicted using a Debye-like model, (cite) from

$$k_{pr} = \frac{1}{V} \int_0^{\omega_{cut}} d\omega DOS(\omega) C(\omega) D_{pr}(\omega), \quad (2)$$

where  $V$  is the system volume,  $\omega$  is the vibrational mode frequency,  $DOS(\omega)$  is the vibrational density of states,  $C(\omega)$  is the vibrational mode specific heat, and  $\omega_{cut}$  is the propagating cut-off frequency, and  $D_{pr}(\omega)$  is the propagating mode thermal diffusivity (see Eq. (4)).(cite) The cut-off frequency  $\omega_{cut}$  identifies the transition from propagating (phonon-like) to non-propagating (diffuson) modes (see Section IV E).<sup>14-18</sup> The propagating contribution  $k_{pr}$  is written as an integral because the finite simulation sizes studied in this work (and others)<sup>14,16</sup> limit the lowest frequency vibrational modes which can be studied, and an extrapolation must be made to the zero-frequency limit.(cite) Eq. (2) can be obtained using the single-mode relaxation time approximation to solve the Boltzmann transport equation for a phonon gas.<sup>37</sup> Assumed in Eq. (2) are isotropy (valid for an amorphous material) and a single phonon polarization,(cite) making the properties a function of the mode frequency  $\omega$  only. The choice of a single phonon polarization (i.e., an averaging of the transverse and longitudinal branches)(cite) does not significantly change the results predicted in this work or others.<sup>14-18,23</sup>

We write Eq. (2) in terms of the mole diffusivities to align with the diffusion theory, which is described later in this section.

We will evaluate Eq. (2)

Under the Debye approximation, which assumes isotropic and linear dispersion (i.e.,  $v_g = v_s$ ), the density of states,  $DOS(\omega)$ , is

$$DOS(\omega) = \frac{3\pi\omega^2}{2v_{s,DOS}^3}, \quad (3)$$

where  $v_s$  is an appropriate sound speed. (cite) Since we use MD simulations, which are classical and obey Maxwell-Boltzmann statistics,<sup>39</sup> we take the phonon and diffuson specific heat to be ~~(a)(b)~~  $k_B$  in the harmonic limit. This harmonic approximation has been shown to be valid for a-Si modeled using the Stillinger-Weber potential at the temperatures of interest here for low-frequency modes. (cite) Taking the classical limit for the specific heat allows for a direct comparison between the MD- and lattice dynamics-based methods and is discussed further in Section V A.

In a disordered system, only the diffusivity of the low-frequency propagating modes can be written as (cite)

$$D_{pr}(\omega) = \frac{1}{3} v_g^2(\omega) \tau(\omega), \quad (4)$$

where the mode group velocity  $v_g(\omega) = v_s$  and  $\tau(\omega)$  is the mode lifetime. (cite) The physical picture is of propagating plane waves which travel with velocity  $v_s$  for a time  $\tau$  before scattering. (cite) An equivalent physical picture in terms of a scattering length is

$$D(\omega) = \frac{1}{3} v_g(\omega) \Lambda(\omega), \quad (5)$$

where  $\Lambda$  is the phonon mean free path (MFP), defined as

$$\Lambda(\omega) = \frac{v_s}{v_g(\omega)} \tau(\omega). \quad (6)$$

In a disordered system, Eqs. and are only valid in the low-frequency, long-wavelength limit. (cite) Because Eq. (4) is only valid at low frequencies, the mode diffusivity  $D$  is the fundamental quantity for modes at all frequencies and is the focus of this work (see Section IV E). (cite) The propagating thermal diffusivity is modeled using

$$D_{pr}(\omega) = B\omega^{-n}, \quad (7)$$

where  $B$  and  $n$  are constants. At low frequencies (long wavelengths),  $v_g = v_s$  is a constant and the scaling of diffusivity with frequency comes from the lifetime,

The lifetime will be modeled using

$$\tau(\omega) = B_* \omega^{-n}, \quad (8)$$

where  $B_s = B/v_s^2$ . For amorphous materials, the scaling exponent  $n$  has been found to be  $2 \leq n \leq 4$  (cite) where  $n = 2$  corresponds to Umklapp scattering<sup>40</sup> and  $n = 4$  Rayleigh scattering from point defects in a crystal.<sup>41</sup> The form of the  $DOS(\omega)$  [Eq. (3)] and  $D(\omega)$  [Eq. (7)] with  $n \leq 2$  ensures that the thermal conductivity Eq. (2) is finite. (cite) The form for  $D(\omega)$  [Eq. (??)] with  $n > 2$  causes the thermal conductivity [Eq. (2)] to diverge in the low-frequency limit as the system size is increased, (cite) which can be fixed using additional anharmonic scattering<sup>14,16</sup> or boundary scattering.<sup>17,18</sup>

For non-propagating modes in the AF diffuson theory,  $D(\omega)$  cannot be written as Eq. (4).<sup>42</sup> The diffuson contribution to thermal conductivity,  $k_{AF}$ , is<sup>14,16</sup>

$$k_{AF} = \frac{1}{V} \sum_{\omega_i > \omega_{cut}} C_i(\omega) D_{AF,i}(\omega), \quad (9)$$

where  $\omega_i$  is the frequency of the  $i$ th diffuson mode,  $C_i(\omega_i)$  is the diffuson specific heat, and  $D_{AF,i}$  is the diffuson diffusivity. Eq. (9) is written as a sum because there are enough high-frequency diffuson modes in the finite-size systems studied in this work (and others).<sup>14,16</sup> Written as an integral, Eq. (??) has the same form as Eq. 2, which can be derived starting with the Kubo theory<sup>18,23,42-44</sup> and taking the limit of zero phonon self-energy.<sup>23</sup> The AF diffusivities are predicted by<sup>42</sup>

$$D_{AF,i} = \frac{\pi V^2}{\hbar^2 \omega_i^2} \sum_{j \neq i} |S_{ij}|^2 \delta(\omega_i - \omega_j) \quad (10)$$

where  $\hbar$  is Planck's constant,  $S_{ij}$  is the heat current operator between vibrational modes  $i$  and  $j$ , and  $\delta$  is the Dirac delta function. The diffusivity of diffusons can be calculated from harmonic lattice dynamics theory.<sup>14,16,42</sup> The heat current operator  $S_{ij}$  measures the thermal coupling between modes  $i$  and  $j$  based on their frequencies and spatial overlap of eigenvectors (see Section IV B and IV D). For Eq. (10),  $S_{ij}$  is directionally averaged because the amorphous materials studied in this work are isotropic. (cite) The diffuson specific heat is taken to be  $C(\omega) = k_B$  to remain consistent with the same assumption for low-frequency propagating modes and the MD- and LD-based methods compared in this work. The implication of this assumption is discussed in Section VA. Now discuss previous work

While predictions for the contributions to the total vibrational thermal conductivity  $k_{vib}$  from propagating ( $k_{pr}$ ) and non-propagating ( $k_{AF}$ ) have been made for a-SiO<sub>2</sub> and a-Si, (cite) no thermal conductivity accumulation functions have been predicted to compare with Regner. (cite) Using lattice dynamics calculations and molecular dynamics simulations

of large-scale (4000 atom models), we predict the inputs to Eq. (1) in Sections IV A, IV B, IV E, and the bulk thermal conductivity  $k_{vib}$  and its contributions  $k_{pr}$  and  $k_{AF}$  in Section V A. Using very large-scale (up to 800,000 atoms) MD simulations, we predict the thermal thermal conductivity  $k_{vib}$  of bulk a-SiO<sub>2</sub> and a-Si to compare with the predictions based on the mode-by-mode properties. For the first time, the MFPs of propagating modes in bulk a-SiO<sub>2</sub> and a-Si are used with a boundary scattering model to predict the thermal conductivity accumulation, which is compared with experimental thin film measurements and broadband FDTR measurements of a-SiO<sub>2</sub> and a-Si in Section V B.

## B. Thermal Conductivity and Diffusivity Limits

To understand the non-propagating contribution  $k_{AF}$ , it is useful to consider a high-scatter (HS) limit for the mode diffusivity,

$$D_{HS} = \frac{1}{3} v_s a, \quad (11)$$

where it is assumed that all vibrational modes travel with the sound speed  $v_s$  and scatter over a distance of the lattice constant  $a$ . (cite) This diffusivity assumption leads to a high-scatter (HS) limit of thermal conductivity in the classical limit<sup>45</sup> *giving*

$$k_{HS} = \frac{k_B}{V_b} b v_s a, \quad (12)$$

where  $V_b$  is the volume of the unit cell and  $b$  is the number of atoms in the unit cell.<sup>46</sup> The advantage is that  $k_{HS}$  is a simple functional form of the macroscopic material properties which can be evaluated with experimental measurements or modeling predictions. While Eqs. (11) and (12) are commonly used to establish a high-scatter limits for diffusivity and thermal conductivity, predictions for a-SiGe alloys<sup>14</sup> and experiments demonstrate that these are not true high-scatter limits. However,  $k_{HS}$  is a good lower limit for the thermal conductivity of a-SiO<sub>2</sub>(cite) and a-Si,(cite) as well as other glasses.(cite)

It was demonstrated by Kittel<sup>suggested</sup> that the thermal conductivity of glasses in the high-temperature limit could be interpreted using a temperature-independent high-scatter diffusivity on the order of Eq. (11).<sup>47</sup> This corresponds to a propagating (phonon) model with MFP  $\Lambda = a$ , too small to justify use of the model. The success of Kittel's theory implies that the dominant modes in most glasses are diffusons and not phonons, and  $k_{vib} \approx k_{HS}$ .<sup>47,48</sup>

*that dominate thermal transport*

*specify that*

*the link to diffusons here is not clear*

is predicted to be close to (quantity?)

For

and a model of a-GeTe, ?

For example, amorphous Lennard-Jones argon is dominated by high-scatter modes,<sup>49</sup> as is a model of a-GeTe,<sup>50</sup> and both their  $k_{vib}$   $\approx k_{HS}$ . For a-SiO<sub>2</sub>,  $k_{vib} \approx 2k_{HS}$ , while it is unclear what the appropriate lattice constant  $a$  should be, making a factor of 2 reasonably uncertain. (cite) For a-Si, the experimentally measured thermal conductivity at 300 K is  $k_{pr} \approx (1 - 6)k_{HS}$ ,<sup>46</sup> indicating that there may be a large contribution from  $k_{pr}$ . We investigate the contributions  $k_{pr}$  and  $k_{AF}$  using detailed atomistic models for a-SiO<sub>2</sub> and a-Si which are described in the next section.

Not  
here

### III. CALCULATION DETAILS

#### A. Sample Preparation

The a-SiO<sub>2</sub> samples are used from Ref. 51 and have size  $N_a = 288$ , 576, and 972 where  $N_a$  are the number of atoms in the supercell sample. These samples were originally prepared using a melt-quench procedure. (footnote) Using the same procedure, larger systems of  $N_a = 2880$ , 4608, and 34,562 were created. The largest sample has  $N_a = 34,562$  and supercell size  $L = 8.052$  nm. All samples were simulated at a density  $\rho = 2350$  kg/m<sup>3</sup>. (cite) The atomic potential used for a-SiO<sub>2</sub> is the modified BKS potential from Ref. 51, except that the 24-6 Lennard-Jones (LJ) potential is changed to a 12-6, which has a negligible effect on the predictions presented in this paper. The LJ potentials use a cutoff of 8.5 Å and the Buckingham potential uses a cutoff of 10 Å. The electrostatic interactions are handled using the Wolf method with exponential parameter  $\eta = 0.223\text{Å}^{-1}$  and a cutoff of 12 Å.<sup>52</sup> (3D remove the metastability, All generated using direct summation)

For a-Si, we use models created by the modified Wooten-Winer-Weaire (WWW) algorithm from Ref. 53. Sample sizes with  $N_a = 216$ , 1000, 4096, and 100,000 were provided. A large sample was created from the  $N_a = 100,000$  sample by treating it as a unit cell and tiling twice in all directions to create an  $N_a = 800,000$  sample with supercell size  $L = 24.81$  nm. All a-Si structures used have  $\rho = 2330$  kg/m<sup>3</sup>, equivalent to the perfect crystal with a lattice constant of  $a = 5.43$  Å. The Stillinger-Weber potential is used for these a-Si samples.<sup>54</sup>

Small samples of a-SiO<sub>2</sub> and a-Si are shown in Fig. 1. Both a-SiO<sub>2</sub> and a-Si samples were annealed at a temperature of 1100 K for 10 ns to remove meta-stability.<sup>16</sup> Amorphous materials have many different atomic (potential energy) configurations with nearly equivalent energies.<sup>16,55,56</sup> The removal of meta-stability is demonstrated by a decrease of the sample's

(4) leading to potential meta-stability during MD simulations.

how? put details in  
main text

is the variable  $N_a$  needed?

[Fig. 1(a)]

atoms (all cubic cells)

size (length of

[Fig. 1(b)] atoms  
size length of  
lattice constant of  
model for atomic interactions

①

potential  
and plateau

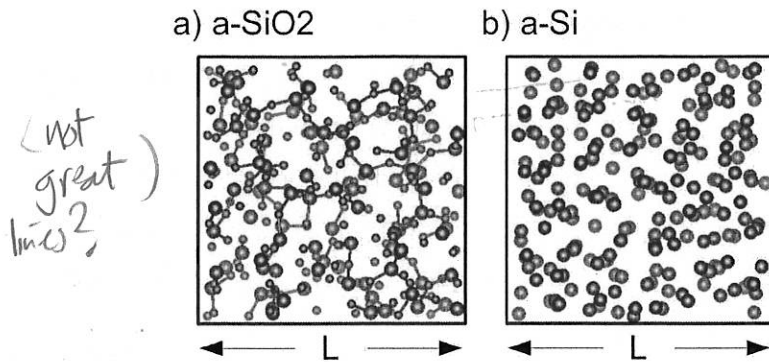


FIG. 1: (a) a sample supercell of a-SiO<sub>2</sub> with  $N_a = 288$  and cell length  $L = 1.597$  nm. Samples up to size  $N_a = 4,608(36,864)$  and  $L = 4.026(8.052)$  nm are used for the LD- and MD-based methods in Sections IV D and IV E. The samples were prepared using a melt-quench technique (see Section III A). (b) a sample supercell of a-Si with  $N_a = 216$  and cell length  $L = 1.597$  nm. Samples up to size  $N_a = 4,096(800,000)$  and  $L = 4.344(24.81)$  nm are used for the LD- and MD-based methods in Sections IV D and IV E. The a-Si samples were prepared using a modified WWW algorithm (see Section III A). Both a-SiO<sub>2</sub> and a-Si structures are visualized using the VESTA package.<sup>57</sup>

potential energy from the pre-annealed configuration. This meta-stability can cause errors when predicting vibrational lifetimes using Normal Mode Decomposition (NMD, see Section IV D).(cite) Q

(footnote) The entire melt-quench procedure is performed at constant volume.<sup>51</sup> Crys-talline silica (c-SiO<sub>2</sub>) is first melted at a temperature of 10,000 K in a cubic simulation cell. The liquid is then quenched instantaneously to 300 K and annealed for 10 ns.

## B. Simulation Details

*0.905 (0.5) fs*

Molecular dynamics (MD) simulations are performed using the disordered a-SiO<sub>2</sub> and a-Si supercells described in Section III A. The MD simulations were performed using LAMMPS<sup>58</sup> with time steps of ~~0.00005~~ 0.00905 (0.0005) ps for a-SiO<sub>2</sub>(a-Si). Ten MD simulations with different initial conditions were run and the predictions from these simulations were ensemble averaged. All MD simulations are first equilibrated in a ~~NVT~~ (constant number of atoms, volume, and temperature) ensemble for  $10^6$  time steps. Data are then collected from simulations in the ~~NVE~~ (constant number of atoms, volume, and total energy) ensemble for  $2^{21}$  *iters*

where time steps are sampled over  $2^8$  time steps.

[i.e., without using Eq. (1)]

The Green-Kubo (GK) method is used to predict the thermal conductivity  $k_{GK}$  (see Section V A) from MD simulations of the largest supercells of a-SiO<sub>2</sub> and a-Si (see Section III A). The  $k_{GK}$  is predicted by window averaging the integral of the heat current autocorrelation function (HCACF). (cite) For a-SiO<sub>2</sub> and a-Si, a interval of the the HCACF integral can be found which is constant within the statistical noise. (cite) Within the errors reported in Fig., the first-avalanche method predict the same value for  $k_{GK}$ . (cite) For  $N_a = 4,608(4,096)$ , the trajectories from the MD simulations used for the GK method are also used with the NMD method to predict the vibrational mode lifetimes for a-SiO<sub>2</sub>(a-Si) (Section IV D).

For the amorphous supercells studied, the only allowed wave vector is the gamma-point (i.e.,  $\kappa = 0$ ), where  $\kappa$  is the wavevector and there are  $3N_a$  polarization branches labeled by  $\nu$ . (cite) Calculation of the vibrational modes at the Gamma point (referred to as Gamma-modes) require the eigenvalue solution of a dynamical matrix of size  $(3N_a)^2$  that scales as  $[(3N_a)^2]^3$ , limiting the system sizes that can be considered to  $N_a = 4,608(4,096)$  for a-SiO<sub>2</sub>(a-Si). The eigenvalue solution is required to predict the vibrational density of states (DOS) (Section IV A) and structure factors (Section IV B), perform the NMD technique (see Section IV D), and perform the AF calculations (see Section IV E). The frequencies and eigenvectors were computed using harmonic lattice dynamics calculations and GULP.<sup>52</sup> The calculation of the AF diffusion thermal diffusivities [Eq. (10)] is performed using GULP and a Lorentzian broadening of  $14\delta\omega_{avg}(5\delta\omega_{avg})$  for a-SiO<sub>2</sub>(a-Si), where  $\delta\omega_{avg}$  is the average mode frequency spacing [ $\delta\omega_{avg} = ()$  for a-SiO<sub>2</sub>(a-Si)]. (cite) For a-Si the broadening used here is within 20% of that used in Ref 16. Varying the broadening around these values does not change the resulting thermal conductivity  $k_{AF}$  significantly (see Section V A).

Why?

other than  
value of  $\delta\omega_{avg}$   
too  
specifi  
here -  
maybe in  
footnotes?

## IV. VIBRATIONAL PROPERTIES

### A. Density of States

In this section, we examine the vibrational frequencies and density of states (DOS) for our models of a-SiO<sub>2</sub> and a-Si. The vibrational DOS is computed by *from*

should be  
introduced  
at Eq. (1)

$$DOS(\omega) = \sum_i \delta(\omega_i - \omega), \quad (13)$$

of width  $100\delta\omega_{avg}$

results

where a unit step function is used to broaden  $\delta(\omega_i - \omega)$ . (cite) The DOS for a-SiO<sub>2</sub> and a-Si are plotted in Fig. 2 using a broadening of  $10\delta\omega_{avg}$  and  $100\delta\omega_{avg}$ . Because of the finite model size, the low-frequency modes are sparse and the DOS can depend on the broadening.<sup>16</sup> We This use a broadening which is large enough to obtain good statistics but also small enough to capture fine behavior extend to low frequencies.

The DOS for a-Si is similar to the DOS of crystalline silicon,<sup>59,60</sup> with pronounced features at mid-range and high-frequencies. The DOS for a-SiO<sub>2</sub> is essentially constant over most of the frequency-range, with a gap at the higher frequencies due to the presence of the oxygen atoms. (cite) There is a clear scaling of  $DOS \propto \omega^{-2}$  for both a-Si and a-SiO<sub>2</sub> at the lowest frequencies. The onset of this scaling occurs at a higher frequency for a-Si than a-SiO<sub>2</sub>. This scaling of the DOS at low frequencies is predicted by the Debye model [Eq. (3)] which is based on a linear, isotropic crystal. (cite) The DOS scaling at the lowest frequencies for a-SiO<sub>2</sub> and a-Si suggest that the modes may be propagating (phonon-like), which is investigated in the following sections.

## B. Structure Factor

Calculating the structure factors of the supercell Gamma modes is a method to test for their propagating (plane-wave) character at a particular wave vector and polarization.<sup>16,61</sup> The structure factor has been used to predict effective dispersion curves of amorphous materials experimentally (cite more)<sup>62</sup> and numerically (cite more).<sup>16,63</sup> The structure factor at a wave vector  $\kappa$  is defined as<sup>61</sup>

$$S^{L,T}(\omega) = \sum_{\nu} E^{L,T}(\nu) \delta(\omega - \omega(\kappa=0)), \quad (14)$$

where the summation is over the Gamma modes,  $E^T$  refers to the transverse polarization and is defined as

$$E^L(\nu) = \left| \sum_b \hat{\kappa} \cdot e(\kappa=0 \frac{b}{a}) \exp[i\kappa \cdot r_0(l=0)] \right|^2 \quad (15)$$

and  $E^L$  refers to the longitudinal polarization and is defined as

$$E^T(\nu) = \left| \sum_b \hat{\kappa} \times e(\kappa=0 \frac{b}{a}) \exp[i\kappa \cdot r_0(l=0)] \right|^2. \quad (16)$$

In Eqs. (15) and (16), the  $b$  summations are over the atoms in the disordered supercell,  $r_0(l=0)$  refers to the equilibrium atomic position of atom  $b$ ,  $l$  labels the unit cells ( $l = 0$  for

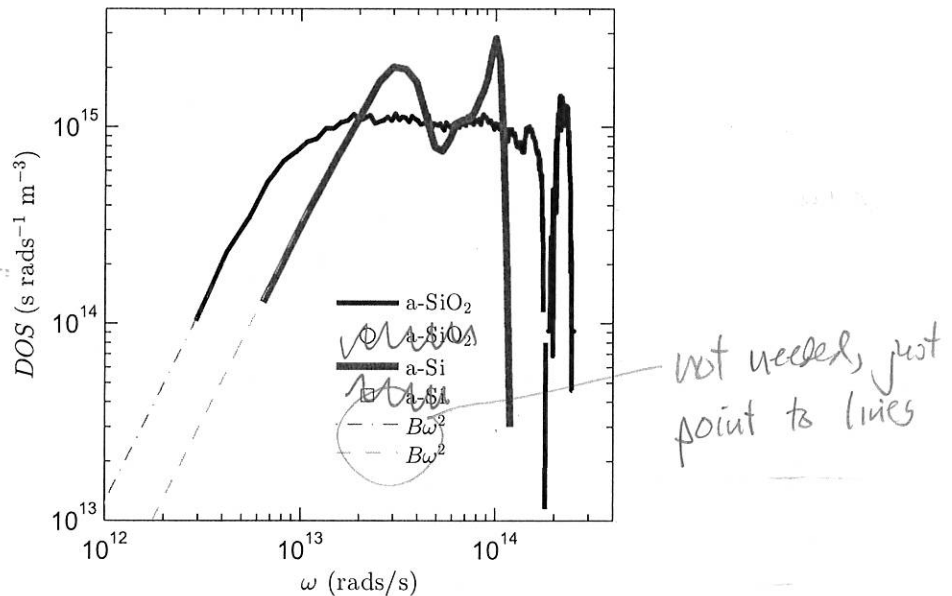


FIG. 2: Vibrational DOS predicted for our models of a-SiO<sub>2</sub> and a-Si using Eq. (13). Both models show a scaling at low frequency  $DOS(\omega) \propto \omega^{-2}$ , which is predicted by the Debye approximation (Eq. (3)) using the transverse sound speeds predicted using various methods (Table I). At high frequency, the DOS of a-SiO<sub>2</sub> shows a plateau and then a sharp feature corresponding to a gap in the vibrational spectrum due to the Si and O bonds.(cite) For a-Si, there are two sharp peaks, which show as small peaks in the predictions of the vibrational mode lifetimes (Fig. 4) and mode diffusivities (Fig. 5).

ok, but in  
main text  
near those  
figures

the supercell),  $\alpha$  labels the Cartesian coordinates, and  $\hat{\kappa}$  is a unit vector. The vibrational mode shape is contained in the  $3N_a$  components of its eigenvector,  $e(\kappa=0 \alpha)$ .(cite)

The structure factors  $S(\kappa)$  are plotted in Fig. 3 for a-SiO<sub>2</sub> and a-Si (left and right panels) for wavevectors along the [100] direction of the supercells. Because of isotropy, the direction is not important and the wavenumber can be considered instead of wavevector.

The wavenumbers are normalized by a maximum wavenumber  $\kappa_{max}$  which corresponds to  $2\pi/a$ , where The length scale  $a$  is 4.8(5.43) Å for a-SiO<sub>2</sub>(a-Si), which is based on the lattice constants of c-SiO<sub>2</sub>(c-Si).(cite)

Mode Frequencies  $[\omega_0(\kappa)]$  and linewidths  $[\Gamma(\kappa)]$  can be predicted by fitting each structure factor

(place fig 3  
closer to  
this text)

peak  $S^{L,T}(\kappa)$  to a Lorentzian function

$$S^{L,T}(\omega) = \frac{C_0(\kappa)}{[\omega_0(\kappa) - \omega]^2 + \Gamma^2(\kappa)}, \quad (17)$$

where  $C_0(\nu)$  is a constant related to the DOS.<sup>64</sup> A dispersion relation is identified by plotting  $\omega_0(\kappa)$ <sup>values</sup> in the middle panel of Fig. 3, where the error bars indicate the linewidths <sup>5(a) and 3(b)</sup>.<sup>65</sup>

For a-Si, the peaks are reasonably Lorentzian for all wavenumbers considered.<sup>65</sup> For a-SiO<sub>2</sub>, the peaks are well-approximated as Lorentzian only at the smallest wavenumbers. For large wavenumber, the structure factor peaks are much less than an order of magnitude larger than the background, and the widths are on the order of the frequency range considered in Fig. 3.(cite) For large wavenumber the structure factor takes on the form of the vibrational DOS.

The low frequency behavior is indicative of propagating <sup>Bogoliubov-like modes</sup> wave numbers. For a-SiO<sub>2</sub> and a-Si, the dispersion is nearly linear at small  $\kappa$  with slight concave-down dispersion at high  $\kappa$ .(cite) For a-SiO<sub>2</sub>, the dispersion is concave-down for the smallest wavenumbers considered, transitioning to a strong concave-up dispersion at intermediate wavenumber. For intermediate  $\kappa$ , the longitudinal dispersion for a-SiO<sub>2</sub> is better described by the so-called "dispersion law for diffusons", where  $\omega \propto \kappa^2$ .<sup>64</sup> This large concave-up dispersion has been observed in various amorphous models<sup>65</sup> including of a-SiO<sub>2</sub>.<sup>66</sup> The dispersion predicted by the structure factors show that a-Si has a near linear, crystal-like dispersion while the dispersion for a-SiO<sub>2</sub> is more diffuson-like,(cite) at least over the range of wavenumber and frequencies considered here. At lower frequencies ( $< 100$  GHz)(cite), experimental measurements of a-SiO<sub>2</sub> show a linear dispersion.

### C. Group Velocity ~~(\*)~~ From p 16

We now use

The DOS and structure factors predicted in Sections IV A and IV B are now used to predict the group velocity of modes at the lowest frequencies for a-SiO<sub>2</sub> and a-Si. In the low-frequency, long-wavelength limit the mode group velocities are the sound speed.(cite) By fitting the DOS from Fig. 2 to Eq. (3), a sound speed is predicted  $v_{s,DOS}$  and reported in Table I. Because the DOS is a mixture of transverse and longitudinal modes only a single sound speed is predicted. Both longitudinal and transverse sound speeds can be predicted from the structure factor.(cite) Sound speeds are estimated from the structure factor peaks

by finite differencing the equation

$$v_s = \frac{\delta\omega_0(\kappa)}{\delta\kappa}, \quad (18)$$

The results for the lowest frequencies

and are shown in Table 1 using the lowest frequency peaks from Fig. 3. The transverse and longitudinal sound speeds of a material can also be predicted from the material's bulk ( $G$ ) and shear ( $K$ ) moduli. (cite) The transverse sound speed is given by (cite) From

$$v_{s,T} = \frac{G^{1/2}}{\rho}, \quad (19)$$

and the longitudinal by

$$v_{s,L} = \frac{4G + 3K^{1/2}}{3\rho}. \quad (20)$$

We use the bulk and shear moduli defined in terms of the elastic constants according to the Voight convention. (cite) The sound speeds calculated from the elastic constants are reported in Table 1. The sound speeds predicted for a-Si in Table 1 are in good agreement with those found in a previous study using a similar model.<sup>14,16</sup> Comment about a-SiO<sub>2</sub> sound speeds with expt and modeling. (cite)

It is clear that the DOS of our models for a-Si and a-SiO<sub>2</sub> are characterized by using the transverse sound speeds, rather than an averaging of the transverse and longitudinal which is commonly used. (cite)

$$v_s = \frac{2}{3}v_{s,L} + \frac{1}{3}v_{s,T}. \quad (21)$$

The values of the transverse sound speeds obtained from the elastic moduli are somewhat larger than the structure factors, which results from an indication of the concave-down dispersion seen at low  $\kappa$ , particularly for a-SiO<sub>2</sub> (Fig. 1). (cite) For a-SiO<sub>2</sub>, the concave-down dispersion also affects the low-frequency DOS, where the predicted sound speed  $v_{s,DOS}$  is less than that predicted from the structure factor and the elastic constants (Table 1). The concave-down dispersion is less pronounced for a-Si, where the sound speeds predicted by all three methods are within five percent of each other.

Under the Debye model (Eq. (3)), the smaller transverse sound speed makes the larger contribution to the DOS which scales as the sound speed cubed. For a-Si, the contribution from longitudinal modes to the Debye DOS is nearly an order of magnitude less than the transverse modes for a given frequency interval (Table 1). For a-SiO<sub>2</sub>, the longitudinal and transverse sound speeds are closer, but the concave-down dispersion is stronger than

This paragraph is too long -  
15 condense down to make the point succinctly

TABLE I: (FIX) Estimated from the elastic constants, the pre-annealed group velocities are  $v_{s,T} = 3,670$ ,  $v_{s,L,elas} = 7,840$  for a-Si and  $v_{s,T,elas} = 2,541$ ,  $v_{s,L,elas} = 4,761$  for a-SiO<sub>2</sub> (see Section IV B).

method	Eqs. (19), (20)	Eqs. (14), (18)	DOS Eq. (3)
<b>a-SiO<sub>2</sub></b>			
transverse	3,161	2,732	2,528
longitudinal	5,100	4,779	
<b>a-Si</b>			
transverse	3,886	3,699	3,615
longitudinal	8,271	8,047	

a-Si (Fig. ).(cite experimental DOS) The intensity of the structure factors are directly proportional to the DOS.(cite) The intensity for the dynamic structure factor of transverse polarizations has been found to be four to five<sup>67</sup> and six to eight<sup>68</sup> times larger than longitudinal polarizations for models of a-SiO<sub>2</sub>, which supports our finding that the DOS is dominated by transverse modes. The transverse sound speed predicted by the DOS  $v_{s,DOS}$  is used for both a-SiO<sub>2</sub> and a-Si throughout the rest of this work and is discussed in Section V C.

$E(\nu)$  and  $E^T(\nu)$

I would start with this paragraph on p 14

For a disordered solid, except for the transverse and longitudinal sound speeds, there is not an accepted method to predict the group velocity of each vibrational mode. While the structure factor gives the frequency spectrum needed to construct a propagating state with pure wavevector  $\kappa$ , the mode spectrum  $E^{T,L}(\nu)$  (Eqs. and ) predicts the plane-wave character of each mode. As shown previously, It is not possible in general to assign a unique wavevector to individual modes, even at low frequency,<sup>14,69,70</sup> which makes predicting individual mode group velocities challenging. Attempts have been made to predict individual mode group velocities,<sup>19,38,45,60,71,72</sup> but it is not clear that these methods are consistent with the predictions made by the structure factor.(cite) In the Cahill-Pohl (CP) model, for example, the group velocity of all disordered modes is the sound speed,  $v_s$ , which is also assumed for the HS model Eq. (??).<sup>45</sup> This assumption is not generally valid for any material.<sup>16,19,38,49,60,71</sup> To treat this problem, we focus on the mode thermal diffusivities and compare predictions from the NMD method (Section IV D) and AF theory in Section IV E.

- due that only low-w modes are propagating in Debye regime, therefore the sound speed  
<sup>16</sup> may be sufficient as no big need for diffusions

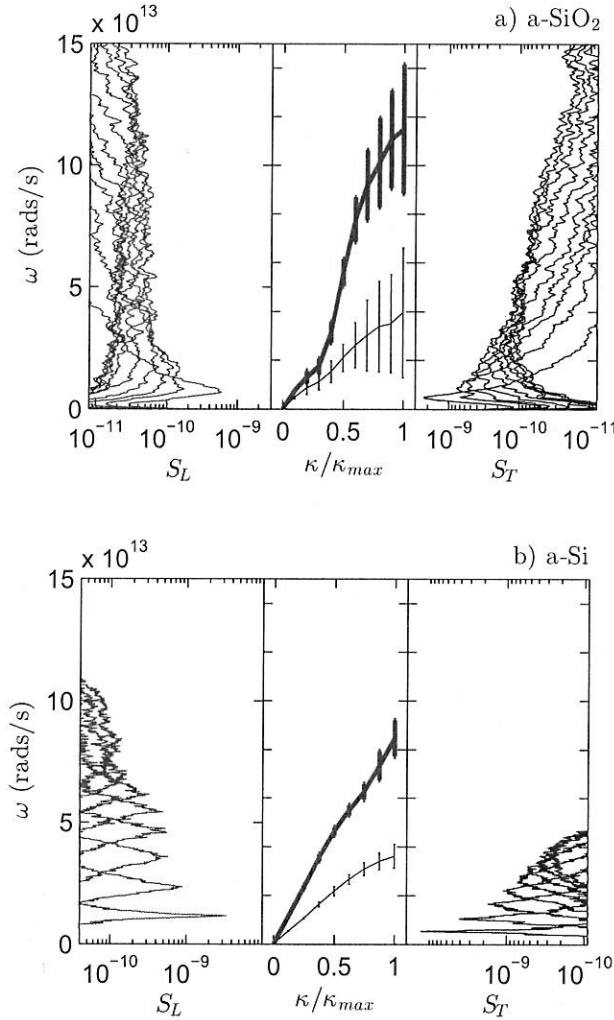


FIG. 3: Longitudinal (left panel) and transverse (right panel) structure factors (Eq. (14)) for a-SiO<sub>2</sub> (top plot) and a-Si (bottom plot). Sound speeds are estimated by finite differencing (Eq. (18)) of the lowest frequency peaks and are reported in Table I. The dispersion for a-SiO<sub>2</sub> is only linear for the lowest frequency, smallest wavenumbers. The dispersion for a-Si is linear over a wider range of wavenumber. Lifetimes are predicted from the widths of the structure factor peaks (Eq. (17)) and are plotted in Fig. 4.

## D. Mode Lifetimes

We now predict the lifetimes of all vibrational modes in our models of a-SiO<sub>2</sub> and a-Si using the MD simulation-based normal mode decomposition (NMD) method.<sup>73-76</sup> The NMD-predicted lifetimes will be compared with the timescales extracted from the structure factor linewidths,  $\tau_{SF} = 1/2\Gamma(\kappa)$  [Section IV B, (Eq. (17))]. The NMD method can predict vibrational lifetimes which are affected by the disorder in the supercell.<sup>19,38,49,77</sup>

In NMD, the atomic trajectories from MD simulations are first mapped onto the vibrational mode coordinate time derivative,<sup>36</sup>

$$\dot{q}(\kappa=0; t) = \sum_{\alpha, b, l}^{3, n, N} \sqrt{\frac{m_b}{N}} \dot{u}_\alpha(b; t) e^{*(\kappa=0)_\alpha^b} \exp[i(\mathbf{0} \cdot \mathbf{r}_0(l)]. \quad (22)$$

Here,  $m_b$  is the mass of the  $b_{th}$  atom in the supercell,  $u_\alpha$  is the  $\alpha$ -component of the atomic displacement from equilibrium,  $\dot{u}_\alpha$  is the  $\alpha$ -component of the atomic velocity, and  $t$  is time. Because the supercells of a-SiO<sub>2</sub> and a-Si are disordered, the NMD method is performed at the wavevector  $\kappa = \mathbf{0}$ . The spectral energy of each vibrational mode,  $\Phi(\nu; t)$ , is calculated from

$$\Phi(\nu, \omega) = \lim_{\tau_0 \rightarrow \infty} \frac{1}{2\tau_0} \left| \frac{1}{\sqrt{2\pi}} \int_0^{\tau_0} \dot{q}(\kappa=0; t) \exp(-i\omega t) dt \right|^2. \quad (23)$$

We choose the frequency domain representation of the normal mode energy because it is less sensitive to any meta-stability of the amorphous structure.(footnote) In an amorphous material, there are many potential energy configurations (atomic positions) which are nearly equivalent in energy. At a sufficient temperature, the meta-stable configurations cause the equilibrium atomic positions to vary in time. This can effect on the prediction of the vibrational mode lifetimes when using the normal mode decomposition method. In the time domain, the average normal mode potential and kinetic energy must be calculated and subtracted from the normal mode energy autocorrelation function.(cite) If the average energy is not specified correctly, unphysically large or small mode lifetimes can be predicted.(cite) (footnote) The vibrational mode frequency and lifetime is predicted by fitting each mode's spectral energy  $\Phi(\nu, \omega)$  to a Lorentzian function,

$$\Phi(\nu, \omega) = \frac{C_0(\nu)}{[\omega_0(\nu) - \omega]^2 + \Gamma^2(\nu)}, \quad (24)$$

where the constant  $C_0(\nu)$  is related to the average energy of each mode and the linewidth  $\Gamma(\nu)$  and is valid when  $\Gamma(\nu) < \omega_0(\nu)$ .<sup>76</sup> The mode lifetime is given by (cite)

$$\tau(\nu) = \frac{1}{2\Gamma(\nu)} \quad (25)$$

The NMD-predicted lifetimes are plotted in Fig. 4 for a-SiO<sub>2</sub> and a-Si. For a-SiO<sub>2</sub>, the mode lifetimes are generally larger than the Ioffe-Regel limit  $\tau = 2\pi/\omega$  (cite) and follow this limit at low frequency. There is no clear evidence for a scaling ~~nowhere~~, which corresponds to a scaling of the diffusivity at low frequency Eq. (7) with  $n = 2$ . At high frequency, the mode lifetimes are roughly constant without definite scaling. There is a peak near  $2 \times 10^{14}$  rads/s, which corresponds to a peak in the DOS (see Fig. 2). The lifetimes predicted from the structure factor fall below the NMD-predicted lifetimes and the IR limit. This is because the structure factor for a-SiO<sub>2</sub> is evaluated for large enough wavenumber that the peaks are not well-approximated as Lorentzian. (cite) Fitting the peaks we find the linewidth (inverse lifetime) to be on the order of the frequency range considered in Fig. 3. Models (cite) and theoretical (cite) predictions show that the structure factor begins to take on the form of the DOS for large enough wavenumber,<sup>23,78</sup> and the linewidths (timescales) are not meaningful. For a-SiO<sub>2</sub>, the NMD and structure factor-predicted lifetimes indicate that the low-frequency modes in our model are not well-characterized as propagating. (cite)

For a-Si, the mode lifetimes show a clear scaling at low frequency ~~as above~~. The lifetimes plateau at higher frequencies, over a wider range of frequencies than a-SiO<sub>2</sub>, with two peaks corresponding to peaks in the DOS (Fig. 2). The plateau of lifetimes at high frequencies has been reported for disordered lattices<sup>49,79</sup> and other models of a-Si.<sup>38</sup> The transition from the low-frequency scaling to the plateau region occurs near  $10^{14}$  rads/s, which corresponds to where the DOS peaks in Fig. 2. Similar behavior has been observed for models of disordered lattices.<sup>49</sup> The lifetimes predicted by the structure factor are in good agreement with those predicted by NMD at low frequencies. Similar agreement has been reported in other models of topologically disordered materials.<sup>80</sup> The longitudinal and transverse polarizations outline the scatter in the NMD-predicted lifetimes. While the DOS at low frequency is dominated by transverse modes, the NMD and structure factor-predicted lifetimes indicate there is some mixture of longitudinal and transverse-like modes. (cite)

The NMD-predicted lifetimes in this work are similar in magnitude to those predicted for previous models of a-Si.<sup>81,82</sup> Fabian and Allen find lifetimes on the order of picoseconds for

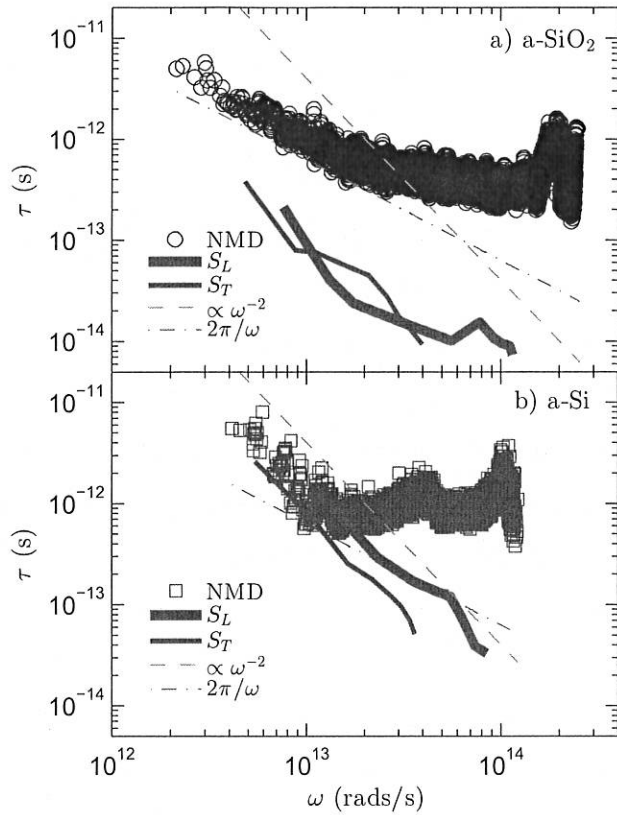


FIG. 4: Vibrational mode lifetimes predicted by NMD [Eq. (25)] and the structure factors [Eq. (17)] for a-SiO<sub>2</sub> (top plot) and a-Si (bottom plot). The IR limit is a lower limit for the NMD-predicted lifetimes, while the lifetimes from the structure factors fall below this limit, particularly for a-SiO<sub>2</sub>. The structure factor lifetimes generally follow a scaling  $\tau \propto \omega^{-2}$  for both systems, while the NMD-predicted lifetimes show a plateau before crossing the IR limit.

a-Si<sup>83</sup> and para-crystalline silicon.<sup>84</sup> A previous study of Tersoff a-Si<sub>3</sub><sub>1</sub> predicted vibrational lifetimes on the order of 100 ps, about ten times the values reported here and in other studies. (cite) It is unclear what the source of this discrepancy is, although the analysis in Ref 19 the NMD method in the time domain. Using the Tersoff potential on the WWW a-Si models in this work we find... Predicted lifetimes are also similar for samples created using a melt-quench technique (see Section ??).

modded using the Tersoff potential  
where meta-stability effects  
can be more strongly  
pronounced.

good to  
do this

## E. Diffusivities

where the DOS  
scales as  $\omega^2$   
(see Fig. 2)

Using the sound speeds predicted from the DOS  $v_{s,DOS}$  (Table I), the NMD-predicted lifetimes are used to predict the mode diffusivities with Eq. (4) and are shown in Fig. (for a-SiO<sub>2</sub> and a-Si). The sound speed is most appropriate for the lowest-frequency modes (see Section IV C). To compare with the NMD predictions, the AF theory is also used to predict the mode diffusivities (see Section IV E), which are shown in Fig. (5).

For a-SiO<sub>2</sub> at the lowest frequencies, the diffusivities scale roughly as Eq. (7) with  $n = 2$ . However this scaling is not definitive for the diffusivities predicted by either method, particularly for the NMD predictions, which is apparent from the scaling of the NMD-predicted lifetimes in Fig. (Because there is no clear transition from propagating to non-propagating modes, we choose  $\omega_{cut} = 4.55 \cdot 10^{12}$  rad/s for Eq. (1) based on the same as that used in Ref. 23 since there is no clear indication of this transition from Fig. ). This choice is discussed in Section V A. The constant  $B$  in Eq. (7) is fit to the AF-predicted diffusivities for  $\omega \leq \omega_{cut}$ .

For a-Si at low frequencies there is a clear scaling of the diffusivities Eq. (7) with  $n = 2$ . The NMD-predicted diffusivities show much less scatter than those predicted by the AF theory, which is due to the finite-size system and the broadening which is required to evaluate Eq. (10).<sup>14</sup> By using a much larger broadening ( $100\delta\omega_{avg}$ ) the scatter in the AF-predicted diffusivities at low frequency can be smoothed, but at the cost of decreasing the diffusivities at intermediate and high frequencies. It is possible that a frequency-dependent broadening may be necessary for a-Si and the AF theory, (cite) but determining this dependence is not clear nor necessary for interpreting the results in this work.

For a-Si, we choose  $\omega_{cut} = 1.16 \cdot 10^{13}$  rads/s and  $B$  so that Eq. (7) is equal to the AF-predicted diffusivity at  $\omega = \omega_{cut}$ . This choice allows Eq. (7) to pass reasonably well through both the AF and NMD-predicted diffusivities. The value of  $\omega_{cut}$  and  $B$  are comparable to those used in Ref. (For a-Si, we also consider a separate scaling for Eq. (7) with  $n = 4$  which is discussed in Section V C. Because this scaling is not clear from the data in Fig. we use  $\omega_{cut} = 1.52 \cdot 10^{13}$  rads/s from Refs. ?? and ?? and choose  $B$  so that Eq. (7) is equal to the AF-predicted diffusivity at  $\omega_{cut}$ . We discuss these choices in Section V C.)

For a-SiO<sub>2</sub>, the mode diffusivities predicted by NMD and AF agree well over the entire frequency range. At high frequencies, the diffusivities do not vary much, except for a peak for the NMD predictions near  $2 \cdot 10^{14}$  rads/s which corresponds to the same peak in the lifetimes

Is this surprising given that you used  $v_s$  for all modes?

Compare both a-SiO<sub>2</sub>, a-Si to HS

(Fig. ). For the AF predictions, the mode diffusivities near  $2 \cdot 10^{14}$  rads/s and at the highest frequencies show a sharp decrease, which is an indication that these modes are localized.(cite)

Both a-SiO<sub>2</sub> and a-Si have a region at higher frequencies where the AF-predicted mode diffusivities are relatively constant. This behavior has been reported for a number of model disordered systems such as disordered lattices<sup>49,64,79</sup>, amorphous solids,<sup>19</sup> and jammed systems.<sup>85,86</sup> For a-Si the NMD- and AF-predicted diffusivities diverge near  $1 \cdot 10^{13}$  rads/s, while the NMD-predicted lifetimes are relatively constant above this frequency.

While diffusons are non-propagating modes whose MFPs are not well-defined, a diffuson MFP can be defined as

or just a length scale?

notation continuing

$$\Lambda_{AF}(\omega) = [3D_{AF,i}(\omega)\tau(\omega)]^{1/2}, \quad (26)$$

where  $\tau(\omega)$  are the NMD-predicted lifetimes. Using this definition,  $\Lambda_{AF}(\omega)$  is found to vary for a-SiO<sub>2</sub> and a-Si between the supercell size  $L$  and the lattice constant  $a$  (see Section III A) for modes with  $\omega > \omega_{cut}$ . Similar MFPs have been estimated for a-Si in previous studies.<sup>14,16</sup> This is in contrast to the MFPs estimated in Ref. 38, which were found to be up to approximately  $70L$ . The reason for this discrepancy is some combination of the predicted lifetimes and the method with which the mode group velocities were estimated.<sup>38</sup>

(see Section IV C)

more than an order of magnitude larger than the system size

## V. THERMAL CONDUCTIVITY

### A. Bulk

To predict the bulk thermal conductivity for our models of a-SiO<sub>2</sub> and a-Si, we use Eq. (1) and the GK method. (46) The GK method for predicting thermal conductivity is relatively inexpensive compared to the NMD and AF methods so large system sizes can be studied (see Section ??). Similarly-large models of a-Si were studied in Ref. 38 using the MD-based direct method to predict thermal conductivity. The details of the GK method are discussed in Section III B.

make this comment in III A

The GK-predicted thermal conductivities  $k_{GK}$  for a-SiO<sub>2</sub> and a-Si are plotted in Fig. 6 for varying system sizes  $L$ . For a-SiO<sub>2</sub>, there is no apparent dependence of  $k_{GK}$  on  $L$ , and the bulk thermal conductivity is estimated to be  $2.10 \pm 0.20$  W/m-K. For a-Si, there is a clear dependence of  $k_{GK}$  on  $L$ . Assuming the DOS has the form of Eq. (3) and the diffusivity  $D$

bulk  
low frequency  
Now?

Comment 4  
Experiment?

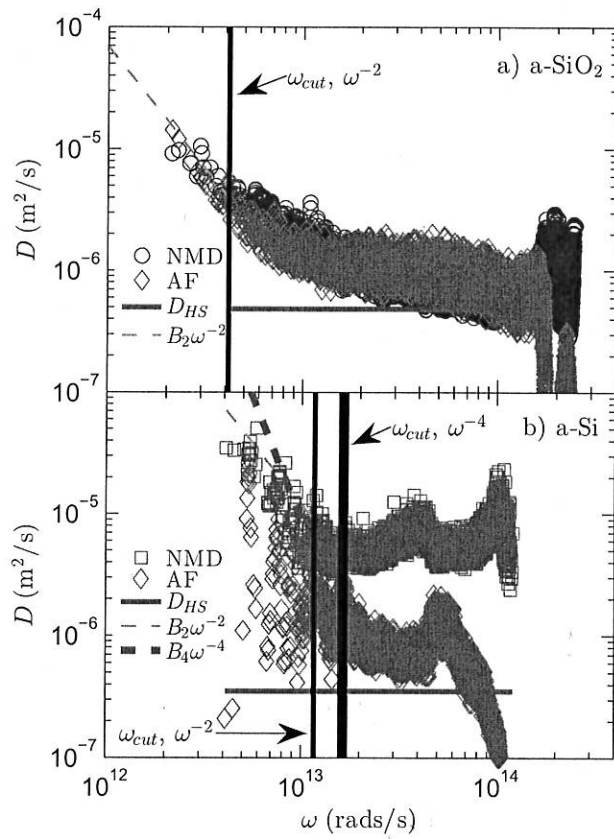


FIG. 5: vibrational mode diffusivities predicted from NMD (using Eqs. (4) and (25) with the sound speed  $v_{s,DOS}$  from Table I) and AF theory (Eq. (10)). Also shown are the extrapolations Eqs. (7) and (??), which are used with Eq. (2) to predict the thermal conductivity accumulations in Fig. 8, and the high-scatter limit Eq. (11).

~~scale as  $\omega^{-2}$~~   
~~scaling is Eq. (7) with  $n = 2$  for the low-frequency modes, the thermal conductivity as a function of the system size takes the form~~ will scale as the inverse of the system size. The bulk value can be found by extrapolating (27) in an infinite system size,

$$\frac{k_{GK}(L)}{k_{bulk}} = 1 - \frac{c_0}{L},$$

where  $k_{bulk}$  is the extrapolated bulk thermal conductivity and  $c_0$  is a constant.<sup>76,87,88</sup> The extrapolation is performed using the three largest system sizes studied, including the tiled 800,000 atom sample (see Section ??). We do not observe that tiling an a-Si model increases the thermal conductivity of a given system size above that predicted by Eq. (27), as was found in Ref. 19 using the MD-based direct method. This is likely due to the small ( $N_a = 512$ ) model used to perform the tiling in that study, while we use a large ( $N_a = 100,000$ )

(100,000 atoms)

model. The success of Eq. (27) for describing  $k_{GK}(L)$  for our model of a-Si is in agreement with the scaling Eq. (7) with  $n = 2$  (Fig. 5 and the Debye scaling of the DOS (Fig. 2). For a-Si, the extrapolated ~~bulk value~~  $k_{bulk} = 1.97 \pm 0.15$  W/m-K

specified in Section

To predict ~~Eq. (1)~~ we use the input parameters  $B$  and  $\omega_{cut}$  and the AF-predicted diffusivities ~~DB(10)~~ obtained in Section IV E. For a-SiO<sub>2</sub>, using Eq. (7) with  $n = 2$   ~~$k_{AF} = 1.92$ ,  $k_{pr} = 0.09$  W/m-K, and  $k_{vib} = 2.01$  W/m-K, which is equal to  $k_{bulk}$  within the errors.~~ Baldi et al. estimated a similar value  $k_{pr} \approx 0.1$  W/m-K for a-SiO<sub>2</sub>.<sup>23</sup> We consider the contribution ~~predicted in this work to be an upper-bound considering the lack of definitive scaling of Eq. with  $n = 2$  (see Fig. ). Within the errors of the predictions,  $k_{pr}$  is not a significant fraction of  $k_{vib}$  for a-SiO<sub>2</sub>.~~

~~Assuming an  $w^{-2}$  diffusivity scaling, we the propagating, diffusion, and total thermal conductivities are If an  $w^{-1}$  scaling is assumed, the diverging conductivity at low frequency is fixed by the use of a simple boundary scattering model based on the Matthiessen rule and the thin-film thickness  $t_f$ ,~~<sup>89</sup>

$$\frac{1}{\Lambda_{eff}} = \frac{1}{\Lambda_{bulk}} + \frac{2}{t_f} \quad \text{put in terms of diffusivity?} \quad (28)$$

Using the largest  $t_f = 80 \mu\text{m}$  from the literature(cite) gives  $k_{pr} = 2.98$  W/m-K. Using the  $w^{-2}$  scaling and  $t_f = 80,000$  nm does not change  $k_{pr}$  within the precision reported. For  $t_f = 50$  nm,  $k_{pr} = 0.22$  W/m-K for  $n = 4$  and  $k_{pr} = 0.34$  W/m-K for  $n = 2$ . For  $n = 4$ , using the same ~~The same  $\omega_{cut}$  was used by Cahill et al. together with a Rayleigh scaling and a boundary scattering model to find  $k_{ph} = 0.31$  W/m-K.~~<sup>15</sup>

In Section II A we approximated the specific heat of the propagating and non-propagating (diffusions) modes by the classical-limit value  $C(\omega) = k_B$ . The full quantum expression for the specific heat is

$$C(\omega) = k_B \frac{\hbar\omega/2k_BT}{\sinh(\hbar\omega/2k_BT)} \quad (29)$$

where  $T$  is the temperature and  $C(\omega/T)_B$  as  $\omega/T$  goes to zero (classical limit).(cite) For a temperature  $T = 300$  K,  $C(\omega/T) = 0.98k_B$  for  $\omega = \omega_{cut} = 1.5210^{13}$  rads/s, the largest  $\omega_{cut}$  used for a-SiO<sub>2</sub> or a-Si in this work. Using the classical limit for specific heat is a good approximation for the modes considered in  $k_{pr}$ , while it is an approximation for the high-frequency modes in our models. For a-SiO<sub>2</sub>(a-Si), the maximum frequency in the model is  $\omega_{max} = 2.48(1.22)10^{14}$  rads/s and  $C(\omega/T) = 0.073(0.47)k_B$ . Thus the quantum effect on  $C(\omega/T)$  affects the contribution  $k_{AF}$  only, which we can consider to be an adjustable

the propagating, diffusion, and total thermal conductivities are 0.073(0.47) and 2.01 W/m-K

what is purpose of these comments?

why make this decision now - could do it before reporting k values, a may be I understand re: g/k - I see the point, but it does not fit from the flow

(Some of this  
text might go  
in intro)

Following the suggestion of kohl and colvin, they  
interpreted the measured value at a given penetration depth  
to be representative of the phonons with a mean free  
path less than that value, allowing for the construction  
of the so-called thermal conductivity accumulation  
function.

Their results  
are plotted  
in Fig. 7  
and 8.

constant in  $k_{vib}$ . Using Eq. (29) gives  $k_{AF} = 1.22(0.96)$  W/m-K for a-SiO<sub>2</sub>(a-Si). This correction brings the overestimate of  $k_{vib}$  for a-SiO<sub>2</sub> into better agreement with experimental measurements by Regner et al. (see Fig.). For a-Si the modified  $k_{AF}$  is closer to the classical-limit value, which does not significantly change the predicted  $k_{vib}$  in Fig. . Because the change in  $k_{AF}$  due to quantum effects are reasonably small, particularly for a-Si, we keep the classical-limit value to compare with the MD-based GK predictions in Fig. . In particular, this allows us to verify that the scaling Eq. (7) with  $n = 2$  describes the low-frequency contribution  $k_{pr}$  for our model of bulk a-Si.

The relative contributions of  $k_{pr}$  and  $k_{AF}$  to  $k_{vib}$  have been estimated from experiments and modeling for a-Si and a-SiO<sub>2</sub>. At 300 K for a-Si modeled by the Tersoff potential,  $k_{ph} \approx k_{AF}$ .<sup>38</sup> Earlier studies using similar models of a-Si to those used in this work find that  $k_{pr}$  is less than half of  $k_{vib}$ .<sup>14,16</sup> Estimates based on experimental measurements have shown  $k_{pr}$  as low as 20%<sup>15,16</sup> and as high as 80%  $k_{vib}$ .<sup>17,18</sup> While predictions for  $k_{pr}$  for a-Si depend on the experimental sample preparations (cite) and the assumed scaling of the low-frequency vibrational diffusivities (see Section II A),(cite) all evidence supports that  $k_{pr}$  is a significant fraction of  $k_{vib}$ .(cite)

For a-SiO<sub>2</sub>, modeling based on experiments show that  $k_{pr}$  is less than 10% of  $k_{vib}$ ,(cite) as is found in the present study. The propagating contribution  $k_{pr}$  can be identified for a-Si in this work and others, both experimentally<sup>11,13,17,18</sup> and numerically<sup>14,16,38,51</sup> using both scalings  $n = 2$ <sup>38?</sup> and  $n = 4$ <sup>14,15,17,18</sup>. for Eq. (7). In the next section we consider both of these scalings when predicting the thermal conductivity accumulation functions.

## B. Accumulation Function

don't use acronym

how the thermal conductivity of a-SiO<sub>2</sub>  
and a-Si films changes with the  
penetration depth associated with  
the heating laser pulse

Recent broadband FDTR experiments by Regner et al. measured the apparent thermal conductivity change with the penetration depth  $L_p$  of the experiments between 40 nm and 1  $\mu$ m.(cite) They argue that the apparent thermal conductivity variation with  $L_p$  represents the accumulated thermal conductivity for propagating modes with MFP less than  $L_p$ . The ~~object in Section IV, we will make~~ ~~based on the results~~ thermal conductivity accumulation functions for a-SiO<sub>2</sub> and a-Si from

define  $\Lambda_{cut}$

$$k(\Lambda_{cut}) = \frac{1}{V} \int_0^{\Lambda_{cut}} kb\bar{D}(\Lambda) DOS(\Lambda) + \frac{1}{V} \sum_{\Lambda < \Lambda_{cut}} kbv_{AF} \Delta_{AF}, \quad (30)$$

For a-SiO<sub>2</sub>, the thermal conductivity of a  $\mu$ m film did not vary  
for penetration depths between  $\text{nm}$  and  $\text{nm}$ , suggesting that any propagating modes  
that contribute to thermal conductivity have mean free paths below  $\text{nm}$ . For a-Si,  
they find ...

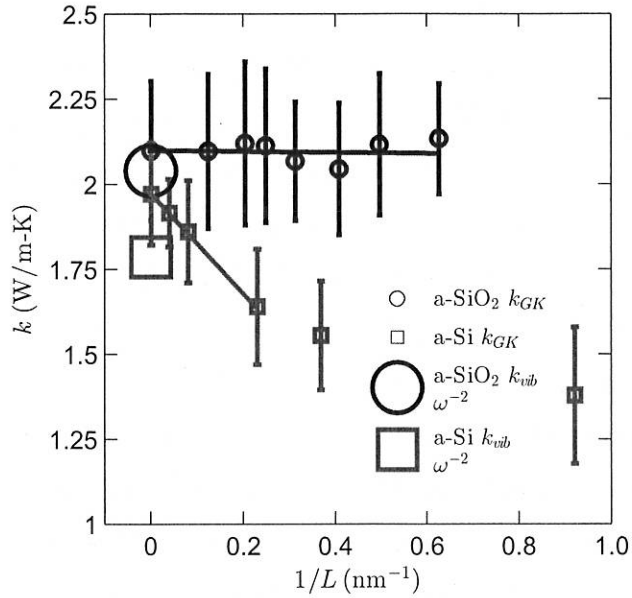


FIG. 6: Thermal conductivities of a-SiO<sub>2</sub> and a-Si predicted using the GK method. For a-SiO<sub>2</sub>, the thermal conductivity is size-independent, indicating there is no important contribution from phonons (Eq. (2)). For a-Si, there is a clear size dependence, which is accounted for by using Eq.

(2) and an  $\omega^{-2}$  extrapolation (Eq. (7), Fig. 5).

(Explain Eq. (30) a little more carefully)

why needed - I feel that it adds consistency

is predicted using our models of bulk a-SiO<sub>2</sub> and a-Si with the boundary scatter model Eq. (30) and are shown in Fig.. The mode MFPs  $\Lambda$  are found using Eqs. and . The

non-propagating diffuson contribution ~~that~~ is considered a constant as discussed in Section

V A.

predicted

The thermal conductivity accumulation function for a-SiO<sub>2</sub> saturates at a MFP of about 10 nm, which is on the order of the finite size of our model (Section III A). This sharp accumulation at small MFPs is in good agreement with the prediction that  $k_{AF}$  is the dominant contribution to  $k_{vib}$  (Section V A). This result is also in accord with the penetration depth-independent thermal conductivity measurements using broadband FDTR.<sup>13</sup> Only the quadratic scaling is considered for a-SiO<sub>2</sub>, which is discussed later in Section V B.

For a-Si, the propagating contribution  $k_{ph}$  is predicted using both scalings Eq. (7) with  $n = 2$  and  $n = 4$ . As discussed in Section V, the  $n = 2$  scaling best describes the propagating contribution for our model of bulk a-Si. The thermal conductivity accumulation functions for both scalings  $n = 2, 4$  are shown in Fig. using  $t_f = 80\mu\text{m}$  with the boundary-scattering

Maybe do  $w^{-2}$  first, discuss, then  $w^{-4}$ .

does not quite make logical sense

feels like too much boundary around

from 2 to 4 - more motivation for H<sub>2</sub>

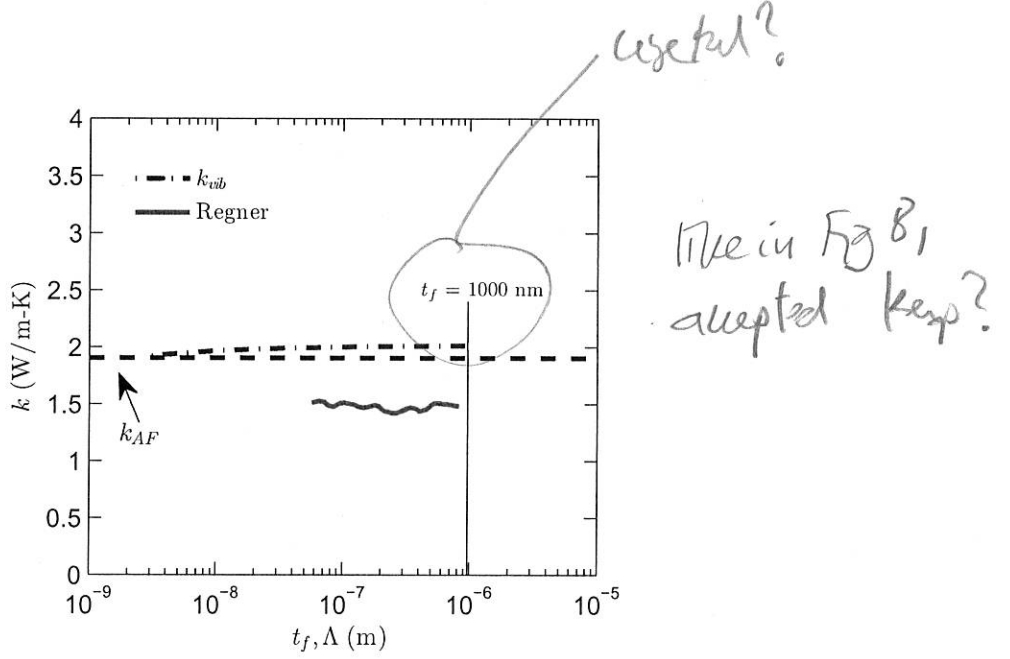


FIG. 7: Thermal conductivity accumulations and thermal conductivities versus film thickness for a-SiO<sub>2</sub> (top plot) and a-Si (bottom plot) from: (i) predictions from this work, (ii) recent broadband measurements of Regner et al, (iii) various experimental measurements for a wide-range of a-Si film thicknesses. While the thermal conductivity predictions for a-SiO<sub>2</sub> and a-Si in this work seem to be well-characterized by Umklapp type scaling of the MFPs (Eq. (7)), this scaling is not able to predict the dramatic increase of thermal conductivity with increasing film thickness from experimental measurements of a-Si thin films.

model Eq. (30). Also shown in Fig. are the broadband FDTR measurements of Regner, which show much sharper accumulations than either  $n = 2, 4$  scalings, particularly for  $t_f = 2\mu\text{m}$  (labeled Regner B in Fig. ). However, the plateau from the measurements of Regner for  $\Lambda < 100 \text{ nm}$  is consistent with our prediction for  $k_{AF}$ . Our predicted  $k_{vib}$  for varying  $t_f$  using Eq. (30) follows roughly the accumulation function, so the experimentally-measured thermal conductivities for varying  $t_f$  are compared directly in Fig. . The experimental measurements for different sample preparations are broadly categorized into (A) HWCVD(cite) and (B) sputtered(cite) techniques. Because of the large variation in experimental measurements, both scalings  $n = 2, 4$  for  $k_{vib}$  passes reasonably well through the measured values.(cite) It is worth noting again that the results from these experiments have been interpreted using both  $n = 2, 4$  scalings.(cite)

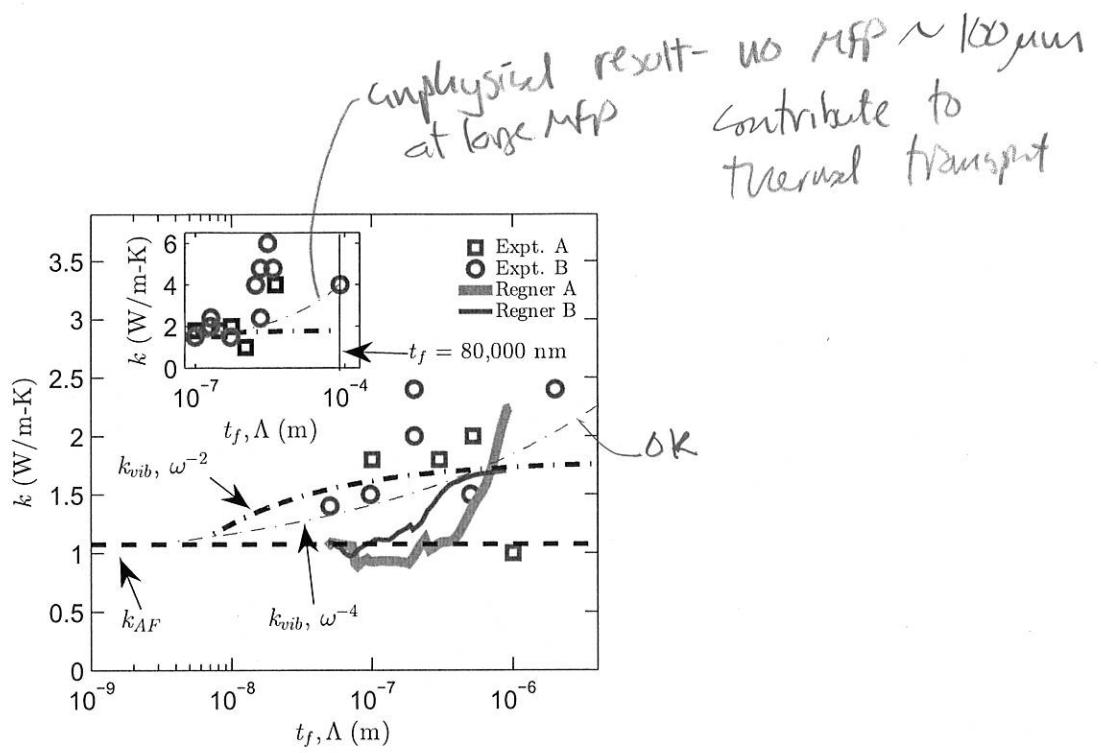


FIG. 8: film thickness dependant thermal conductivity of a-Si from experiment.

### C. Discussion

*does this information need its own section, or can it be integrated into earlier sections?*

The transverse sound speed predicted for our model of a-SiO<sub>2</sub> is about 85% of that predicted by the other methods used in the present study and that measured by experiment.<sup>17</sup> While using a smaller transverse sound speed leads to an underprediction of the mode diffusivity scalings (Eq. (4), Fig. 5), it leads to an overprediction of the DOS (Eq. (3)). Holding all other input parameters in Eq. (1) constant, a smaller sound speed leads to a larger  $k_{pr}$  prediction because the DOS scales as  $DOS(\omega) \propto 1/v_s^3$ . In this sense we can regard the prediction for  $k_{pr}$  from our model of a-SiO<sub>2</sub> with reduced transverse sound speeds as an upper bound. The overestimate of the bulk thermal conductivity predicted for our model of a-SiO<sub>2</sub> can be corrected. Our model confirms that propagating modes do not contribute significantly to the thermal conductivity of a-SiO<sub>2</sub>.

For a-SiO<sub>2</sub>, previous experimental studies have estimated that the contribution  $k_{pr}$  is negligible.<sup>23,90</sup> Using our model of a-SiO<sub>2</sub>, we also find the low-frequency propagating contribution to be negligible (Section V B). While experiments show there is a cross-over region for the low-frequency diffusivity scaling from  $n = 2$  to  $n = 4$  scaling,<sup>22,26</sup> the propagating contribution was still negligible. The cross-over region from  $n = 2$  to  $n = 4$  observed in experiments for a-SiO<sub>2</sub> occurs in the frequency range  $4.610^9$  to  $1.5210^{10}$  rads/s,<sup>22</sup> and  $3.0410^{11}$